

FeSHI: Feature map Based Stealthy Hardware Intrinsic Attack

TOLUPE A. ODETOLA¹, FAIQ KHALID², TRAVIS C. SANDEFUR¹, HAWZHIN MOHAMMED¹ AND SYED RAFAY HASAN.¹

¹Department of Electrical and Computer Engineering, Tennessee Technological University, Cookeville, TN 38505 USA

²Department of Computer Engineering, Technische Universität Wien (TU Wien), Vienna, Austria

arXiv:2106.06895v1 [cs.CR] 13 Jun 2021

ABSTRACT Convolutional Neural Networks (CNN) have shown impressive performance in computer vision, natural language processing, and many other applications, but they exhibit high computations and substantial memory requirements. To address these limitations, especially in resource-constrained devices, the use of cloud computing for CNNs is becoming more popular. This comes with privacy and latency concerns that have motivated the designers to develop embedded hardware accelerators for CNNs. However, designing a specialized accelerator increases the time-to-market and cost of production. Therefore, to reduce the time-to-market and access to state-of-the-art techniques, CNN hardware mapping and deployment on embedded accelerators are often outsourced to untrusted third parties, which is going to be more prevalent in futuristic artificial intelligence of things (AIoT) systems. These AIoT systems anticipates horizontal collaboration among different resource constrained AIoT node devices, where CNN layers are partitioned and these devices collaboratively compute complex CNN tasks. This horizontal collaboration opens another attack surface to the CNN-based application, like inserting the hardware Trojans (HT) into the embedded accelerators designed for the CNN. Therefore, there is a dire need to explore this attack surface for designing the secure embedded hardware accelerators for CNNs. Towards this goal, in this paper, we exploited this attack surface to propose an HT-based attack called FeSHI. Since in horizontal collaboration of RC AIoT devices different sections of CNN architectures are outsourced to different untrusted third parties, the attacker may not know the input image, but it has access to the layer-by-layer feature maps information for the assigned sections of the CNN architecture. This attack exploits the statistical distribution, i.e., Gaussian distribution, of the layer-by-layer feature maps of the CNN to design two triggers for stealthy HT with a very low probability of triggering. Also three different novel, stealthy and effective trigger designs are proposed. To illustrate the effectiveness of the proposed attack, we deployed the LeNet and LeNet-3D on PYNQ to classify the MNIST and CIFAR-10 datasets, respectively, and tested FeSHI. The experimental results show that FeSHI utilizes up to 2% extra LUTs, and the overall resource overhead is less than 1% compared to the original designs. It is also demonstrated on the PYNQ board that FeSHI triggers the attack vary randomly making it extremely difficult to detect.

INDEX TERMS Convolutional Neural Network, CNN, Hardware Security, Edge Intelligence, AIoT, FPGA, Hardware Trojan, Hardware Intrinsic Attack

I. INTRODUCTION

Many Edge Intelligence (EI) based applications require the deployment of Convolutional Neural Networks (CNNs) on Resource-Constrained (RC) Internet of Things (IoT) devices [1]. More recently, Artificial Intelligence of Things (AIoT) also warrants RC devices to compute CNN. Due to design flexibility through partial reconfiguration [2]–[6] and fast prototyping [7] [8], small-scale Field Programmable Gate Arrays (FPGAs) [9] are being used to deploy CNNs on RC devices in AIoT, especially for EI based applications [1].

However, it is very challenging to achieve efficient deployment of CNNs on small-scale FPGAs. Therefore, to achieve resource efficiency, short time-to-market, and state-of-the-art implementation, the deployment of pre-trained CNN on hardware accelerators can be outsourced to untrusted third parties, which provide soft IPs or hard IPs (in the form of bitstream files for FPGA designs) of the deployed CNN. Although outsourcing the CNN deployment achieves the required goal, it comes with security risks such as malicious

hardware insertions, which can be stealthy by nature [10].

Recently, various hardware Trojans (HTs) insertion techniques in CNNs have been explored, but most of them are applicable under the following assumptions:

- These techniques require full access to the CNN architecture to evaluate the triggering probability, stealthiness, and resource utilization (comparing them with design constraints) of their attacks [11]–[14].
- Some of the techniques require a pre-defined sequence, where a sequence of events serves as the trigger for the attack [15]. This sequence of events also requires knowledge of the full CNN architecture, and in the absence of the information about any layer, especially the initial layer and/or the last layer, there is a high probability that the sequence of events may never occur.
- Some of the techniques require weight manipulation, which requires a change in the values of the weights of the CNN to achieve misclassification that can easily be detected using model integrity analysis [16].

In futuristic AIoT systems it is possible that RC AIoT devices collaborate among themselves to perform complex CNN tasks solely using RC devices. This is called horizontal collaboration among RC AIoT devices for edge task offloading [18]–[21]. This collaboration will enable many future applications such as real-time video analytics on edge nodes, natural language processing via collaboration of solely RC AIoT devices, etc. In such scenarios, most of these HT attacks are not applicable due to partitioning of CNN among difference RC devices for horizontal collaboration. Moreover, most of the approaches adopted in state-of-the-art hardware/firmware Trojan attacks on hardware accelerator based CNN inference is focused on the deployment of CNN on a single FPGA with access to the complete CNN pipeline [12], [15], [17]. Table 1 summarizes these differences in the state-of-the-art HT insertion techniques.

To address some of these attacks, defense techniques such as [22] is proposed, which is a trigger approximation-based Trojan detection framework. It searches for triggers in an input space and also detects Trojans in a feature map space. Gao et. al [23] proposes a STRIP defense methodology that turns the strength of an input-agnostic trigger into a means of detecting Trojans at run-time. Doan et. al [24] proposes Februs that neutralizes Trojan attacks on Deep Neural Network (DNN) systems at run-time.

Partitioning of CNN with horizontal collaboration among RC AIoT device [18]–[21] or via vertical collaboration [25] [26] is also considered as an alternative approach to defend attacks. This is because partitioned CNN acts like a distributed network hence it contains the inherent security feature of such networks. Moreover, with partitioned CNN on multiple FPGAs, 3PIPs will not have access to the full CNN pipeline rendering current attack techniques invalid. However, partitioning CNNs on multiple FPGAs can also pose security concerns.

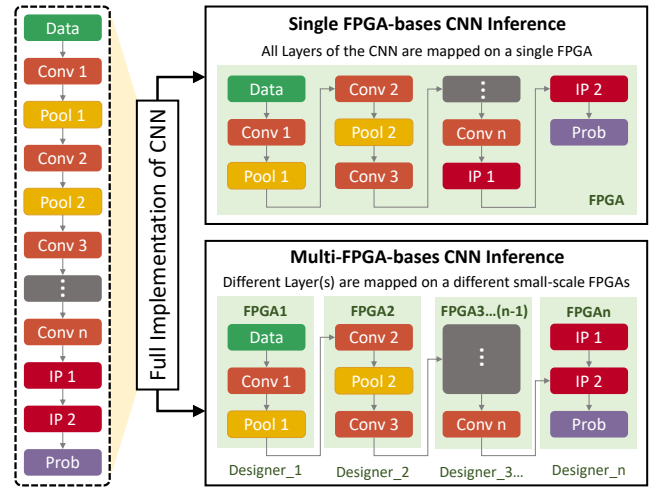


Figure 1: A figurative comparison between single FPGA-based CNN inference and multi-FPGA-based CNN. In single FPGA-based inference, all CNN layers are implemented on an FPGA, and the attacker has access to the complete CNN architecture. On the other hand, in multi-FPGA-based inference, full CNN is divided into multiple different partitions as seen in horizontal offloading, where different third-party IP designers can design each partition. These partitions can be mapped on multiple FPGAs. Note, in multi-FPGA-based inference attacker does not have access to the complete CNN architecture. Hence, the attacker requires an approach that does not require the knowledge of complete CNN architecture.

It is possible that one or more of these FPGA devices are malicious and the CNN deployment on FPGA may be compromised. However, since the malicious devices do not have access to the complete network or ground truth therefore coming up with stealthy and effective hardware attack is challenging. In this paper, we investigate and demonstrate that an attacker may carry out an attack on the CNN while not having complete knowledge of CNN architecture and training or testing dataset. It is worth mentioning here that though the attacker does not have access to the training dataset, nonetheless, it may still be provided with a feature map-based dataset (FM-Dataset) to verify the functional correctness of the hardware. Please note, it is not the traditional validation dataset as provided along with the training dataset for any supervised machine learning techniques.

A. MOTIVATIONAL CASE STUDY

To investigate the viability of the above-mentioned attack, we need to explore whether the small-sized FM-Dataset, with a possible payload in only one of the partitioned CNN layers, can lead to an effective and stealthy attack or not. To answer this we postulate two hypotheses and performed two experiments to confirm the validity of our hypotheses:

Hypothesis 1: A small-sized FM-Dataset can provide an adequate estimate of the statistical attributes of the complete dataset

To investigate this hypothesis, we take 100 images from

Table 1: A brief comparison of the state-of-the-art HT Insertion techniques for CNN

Features / Assumptions	[11]	[12]	[13]	[14]	[15]	[16]	[17]	FeSHI
Access to full CNN architecture to evaluate the triggering probability	✓	✓	✓	✓	✓	✓	✓	×
Pre-defined sequence for designing a trigger	×	×	×	×	✓	×	×	×
Weight manipulation	×	×	×	×	×	✓	×	×
Number of FPGAs / resource-constrained IoT devices for the CNN Inference	one	one/multiple						

the MNIST dataset (as our ground truth) as input into LeNet CNN shown in Fig. 2. The feature maps of the first fully connected layer (ip1 in Fig. 2) are aggregated and the Gaussian distribution plotted. This is repeated for 50 images from the MNIST dataset and compared with the ground truth. From Fig. 2, we observed that the behavior learned from the larger dataset is very similar to the behavior learned using a smaller dataset. For example, Fig. 2 shows the histogram plot of aggregated result of convolution of $(100 \times 84 \times 1)$ input vectors against $(50 \times 84 \times 1)$. The plots show similar Gaussian distribution and statistical attributes in terms of range, mean and standard deviation with a 50% reduction in the dataset (from 100 images to 50 images). These histograms show that the range of values (RoVs) on the x - axis remains very similar for the two cases (only 2.73%). Hence with this result, we validate our hypothesis. In the actual trigger design, we propose to exploit this similarity of RoVs.

Hypothesis 2: A change in the feature map of a particular layer can alter the distribution of the CNN layer leading to misclassification

To demonstrate this, we experimented by rounding down a random amount of values across all the channels in the feature map of the layer of interest to zero (in this case convolution layer). For example, Fig. 2 illustrates the histogram plot of aggregated result of the convolution of $(10 \times 16 \times 12 \times 12)$ input vectors (10 indicates the number of feature maps) with $(16 \times 5 \times 5)$ weight matrices before and after the rounding down half of the elements of the resulting feature maps. The result shows similar statistical attributes with small differences in the Range, mean and standard deviations despite the drastic change in the shape of the Gaussian distribution of the feature map that can serve as input to subsequent layers. Due to the change in Gaussian distribution, we conclude that it is worth exploring to see the effect of such an analysis on complete CNN. Hence, this toy example inspired us to proceed with this approach for the design of a stealthy payload.

B. RESEARCH CHALLENGES

The design of an attack targeted at CNN inference on multiple FPGAs leads to the following research challenges:

- How can we scientifically implement a stealthy attack trigger, based on the statistical attributes of a CNN layer, without access to the full CNN architecture?
- How can we design a payload that will cause misclassification at the final output of CNN, having access to only one or few of the CNN partitioned layers in a horizontal collaboration based AIoT systems?

C. NOVEL CONTRIBUTIONS

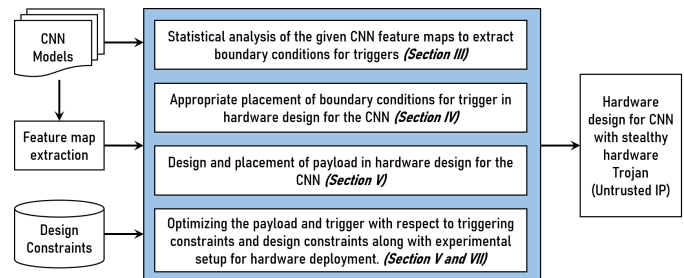


Figure 4: FeSHI attack methodology showing the steps in the deployment of CNN models that involves the output feature map extraction and analysis. The analysis shows the selection of triggering boundary conditions (TBCs) and insertion into the CNN hardware design, payload design and optimization.

To address the above research challenges, we propose a novel Trojan attack methodology for FPGA-based CNN inference called FeSHI (Feature map Based Stealthy Hardware Intrinsic Attack). The FeSHI methodology shown in Fig. 4. Our contributions include the following:

- We propose an attack that triggers at rare occurring events without requiring the complete knowledge of CNN architecture and with no access to weights (except for the partitioned layer(s) that attacker is been provided with). The triggers are designed based on the statistical exploitation of the CNN feature maps to identify vulnerable triggering boundary conditions (TBCs). In this work, TBCs are a range of values that lie beyond the 3σ values of a distribution. (See Section III and IV).
- We also propose a dynamic payload mechanism to further improve the stealthiness of the attack (if the defender tries to come up with test-vectors to detect hardware attacks due to such rarely occurring events).

The evaluation of our proposed FeSHI attack is carried out on Xilinx PYNQ FPGA board (ZYNQ 7020). The experiment test bench shows the following:

- FeSHI proved to be very stealthy by requiring less than 1% additional hardware resources with less than 1% addition to the latency (See Section VI)
- Misclassification (associated payload) can be achieved (after activation) with the attack placed in any of the CNN layers despite limited information about the position of the layer in the CNN architecture on multiple FPGAs.

II. PRELIMINARIES

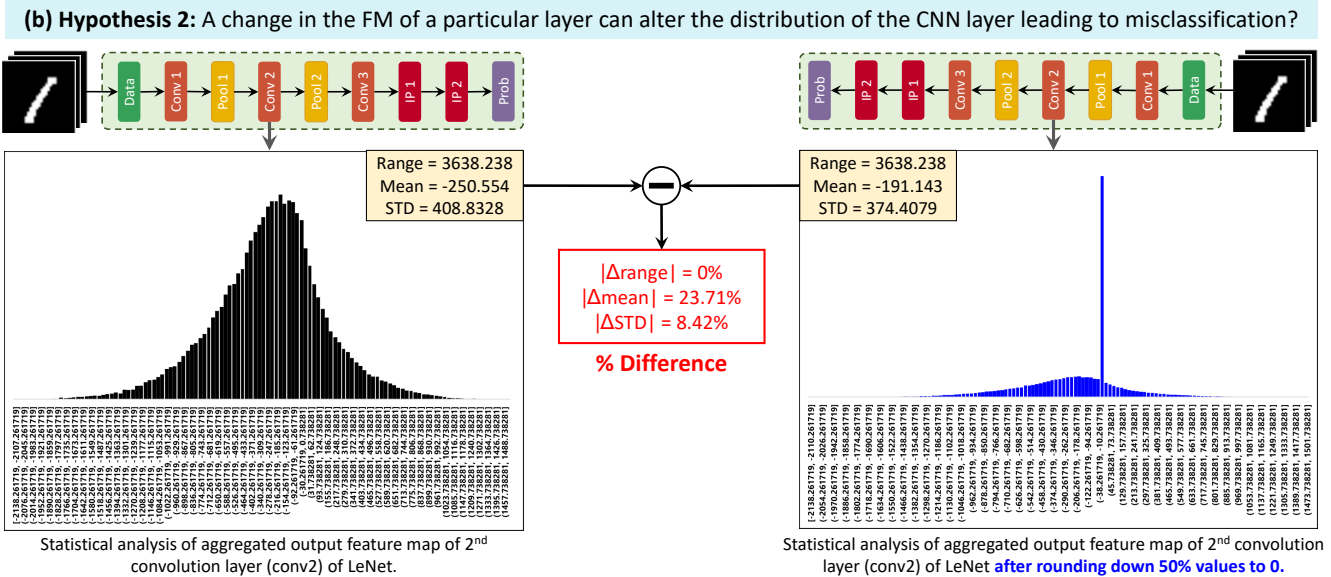
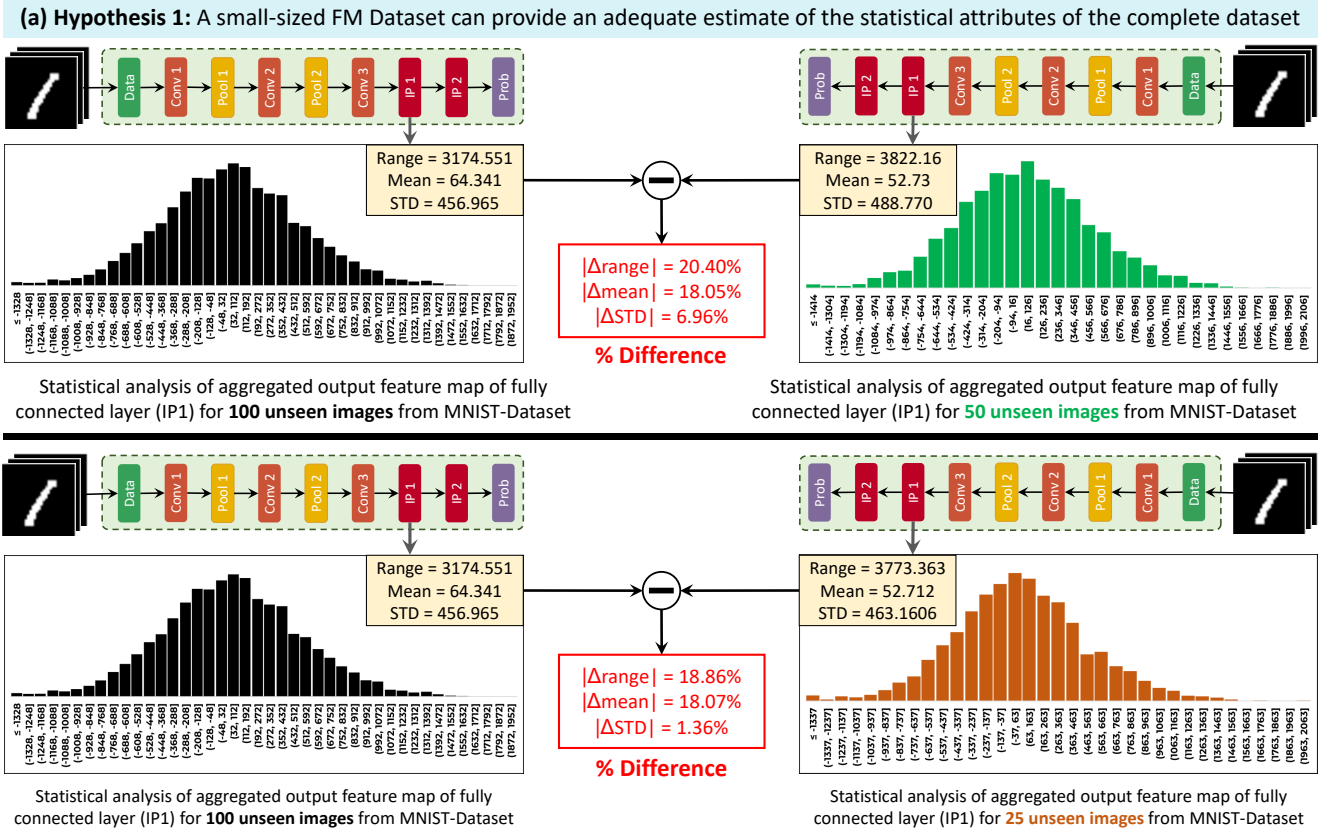


Figure 2: (a) **Hypothesis 1 (Feature map analysis)**: Gaussian distribution plots of aggregated output feature map of the fully connected layer (ip1) layer of LeNet CNN model shown in Fig. 3) in response to 100 and 50 MNIST images, respectively. The plots depict that the Gaussian plot of the response to 50 MNIST images similarity to the plot in response to 100 MNIST images. The plots show an approximate estimate in terms of Range, Mean and Standard deviations. (b) **Hypothesis 2**: Change in the Gaussian distribution of the output feature map of second convolution layer of LeNet (conv2) layer of LeNet CNN model shown in Fig. 3) as a result of rounding down 50% of the values of the feature maps. The plot shows similar statistical attributes in range, mean and standard deviation despite drastic changes in the Gaussian distribution plot.

A. THREAT MODEL

The threat model adopted in this paper follows a gray-box attack where the adversary only has limited knowledge

about the CNN architecture. It is assumed that the attacker has no knowledge of the testing and validation data sam-

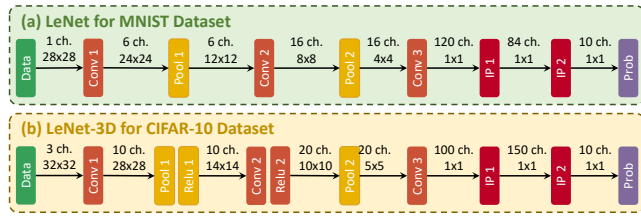


Figure 3: CNN models used in experiments, (a) LeNet trained and tested on the MNIST Dataset (b) LeNet-3D trained and tested on the CIFAR-10 dataset.

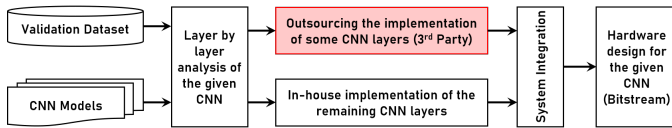


Figure 5: Overview of the design time mapping of CNN Model showing compromised outsourced layers by 3PIPs bitstreams integrated trusted in-house implementation of trusted layers.

ples required for the supervised machine learning of CNN models. This threat model assumes that the CNN can be partitioned into different blocks by employing horizontal offloading, as alluded in Fig. 1 and outsourced to different third parties. In this attack, the attacker has no access to the full CNN layers (specifically the first and final layers which are assumed to be implemented at a trusted IP integration facility - referred to as In-house implementation in Fig. 5), rather the attacker has access to only partial layers. The attacker can perform layer-by-layer analysis on the outsourced partial layers they have access to. We assume that the 3PIP vendors are not trustworthy as shown in Fig. 5, and 3PIPs may contain Hardware Trojan. The attacker provides the CNN hardware design as a bitstream file to the trustworthy project owner or system IP integrator (for single or multi-FPGA CNN deployment).

Fig. 5 depicts the trusted and untrusted aspects of the CNN hardware design. The 3PIP designer has access to the untrusted sections in the IP generation. This work also assumes that for functional/behavioral verification purposes, a FM-Dataset is provided to the 3PIP designer [27], without knowledge or access to the first or final layers.

B. CNN PARAMETER NAMING CONVENTION

Fig. 6 shows a depiction of 3D convolution between an input image I and weights matrix (W_0, \dots, W_k). In this paper, we provide several techniques pertaining to the attack trigger and payload. To understand this paper better, it is pertinent that we define our parameters.

- n_i : Number of input image channels.
- w_i : Number of columns of the input image.
- h_i : Number of rows of the input image.
- w_k : Number of columns of the weight matrix.
- h_k : Number of rows of the weight matrix.
- c_k : Number of the weight matrix.
- w_o : Number of columns of the output feature map.

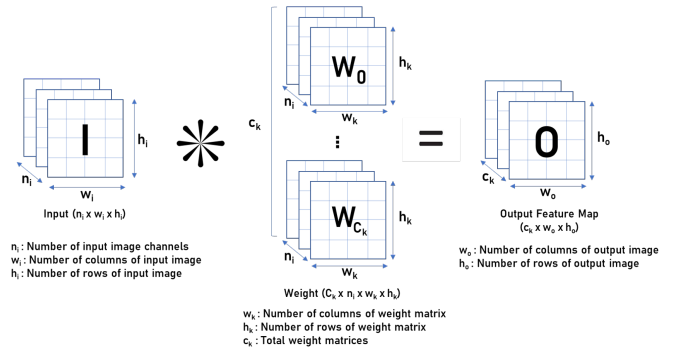


Figure 6: Conceptual representation for dimensions of convolution showing the naming conventions used in this paper

- h_o : Number of rows of the output feature map.

III. FEATURE MAP BASED STEALTHY HARDWARE INTRINSIC (FeSHI) ATTACK

FeSHI makes use of statistical attributes of the Gaussian distribution of the feature maps of CNN layers to investigate rarely occurring range of values (RoVs) for the design of a stealthy hardware intrinsic attack. This section provides the premise of the FeSHI attack's methodology and gives an overview of the attack methodology.

A. METHODOLOGY PREMISE

In CNNs, convolution layers are the most computation-intensive while the fully connected layers are most memory demanding [28]. CNN architectures are designed such that layer-by-layer outputs (feature maps) of previous layers serve as inputs to subsequent layers to achieve classification as shown in Fig. 1.

Feature Maps Follow Gaussian Distribution

To achieve a successful implementation of this attack, without losing generality we consider a convolution layer:

let I be an input vector of shape $n_i \times h_i \times w_i$

let W be a kernel matrix of shape $c_k \times n_k \times h_k \times w_k$

let F be the feature map of the convolution layer of shape $c_k \times w_o \times h_o$

Hence:

$$I \otimes W = F \quad (1)$$

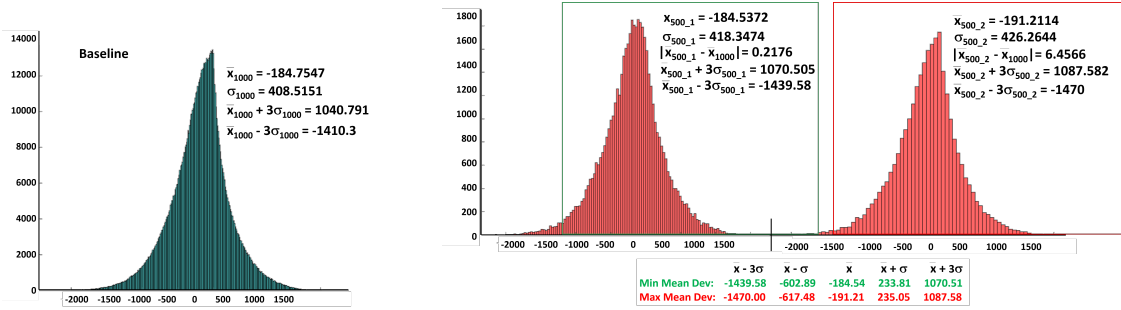
where \otimes represent convolution operation

Therefore:

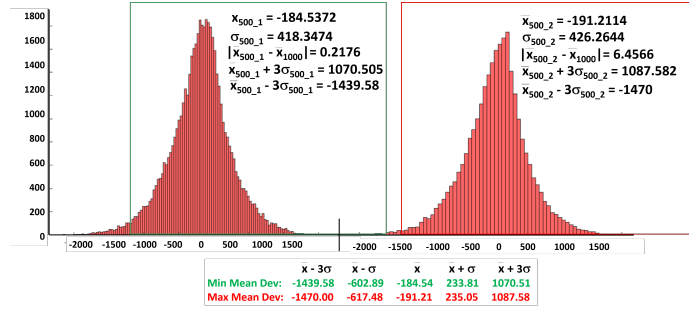
$$(n_i \times h_i \times w_i) \otimes (c_k \times n_k \times h_k \times w_k) = (c_k \times w_o \times h_o) \quad (2)$$

Many common CNN frameworks make use of Xavier (Glorot) [29] as the default weight initializers [30] for training CNN architectures [31]. The weights from Xavier initializers follow a Gaussian distribution [32]. Input images or feature maps also follow Gaussian distribution [33]. Hence:

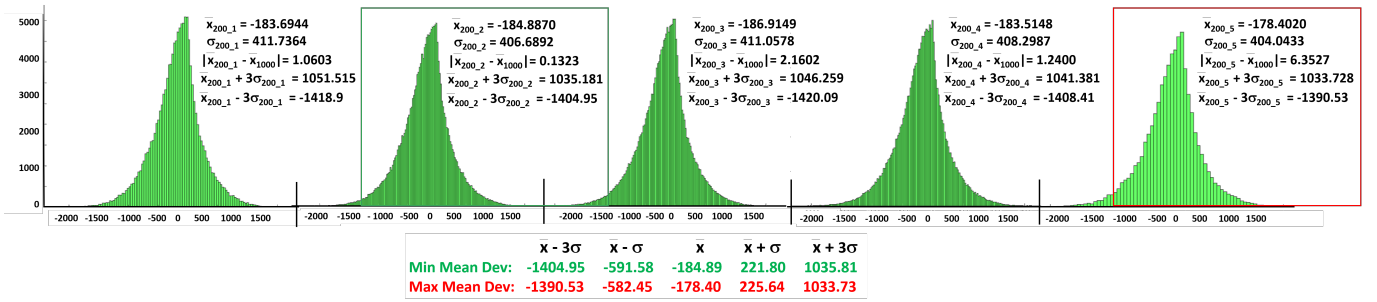
$$W \sim \mathcal{N}(\mu, \sigma^2) \quad (3)$$



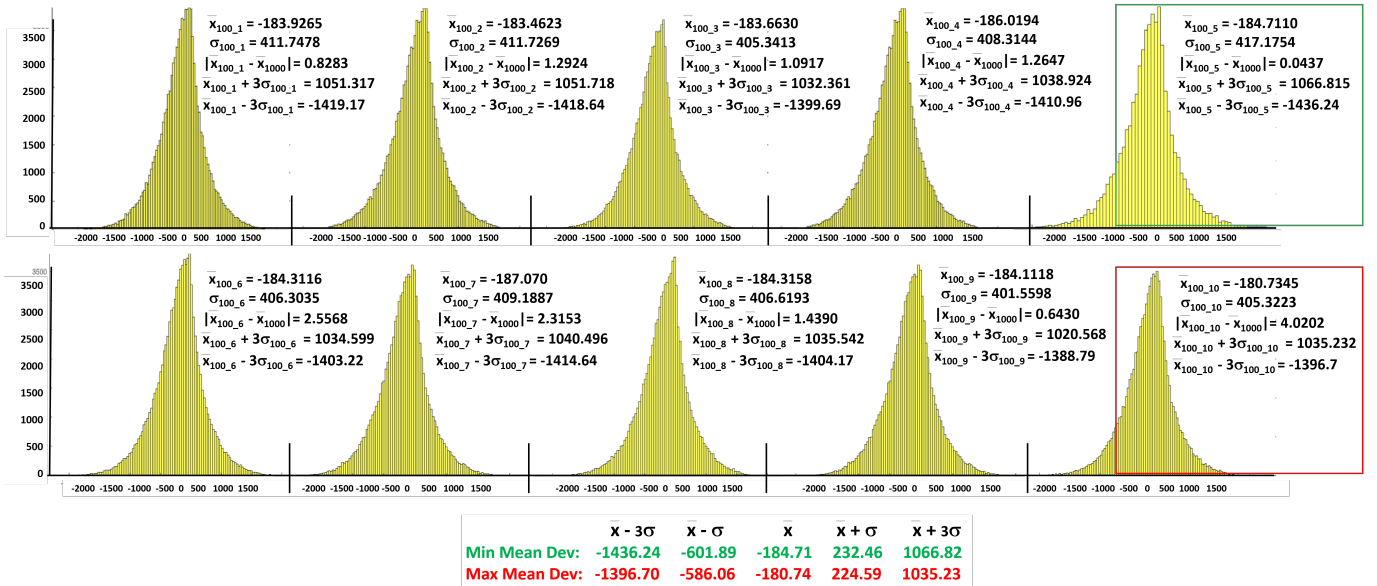
(a) Gaussian distribution, mean, standard deviation and 3σ values of *conv1* output in response to 1000 input MNIST images (Baseline) for 1000 input vectors



(b) Gaussian distribution, mean and standard deviation for 2x500 input vectors and also showing plots with the maximum (in Red box) and minimum (in Green box) mean deviation of 3σ values of *conv1* output for the 2x500 MNIST images when compared with baseline. It can be seen that even the maximum 3σ deviation, which helps this technique in defining RoVs (see Section IV), is within 4.50% of the baseline values.

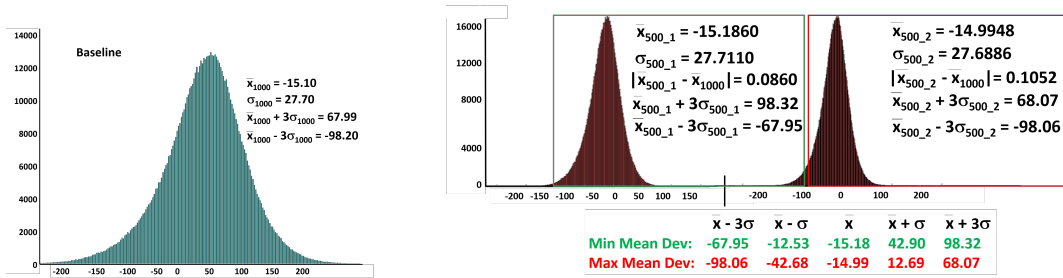


(c) Gaussian distribution, mean and standard deviation for 5x200 input vectors and also showing plots with the maximum (in Red box) and minimum (in Green box) mean deviation of 3σ values of *conv1* output for the 5x200 MNIST images when compared with baseline. It can be seen that even the maximum 3σ deviation, which helps this technique in defining RoVs (see Section IV), is within 1.40% of the baseline values.



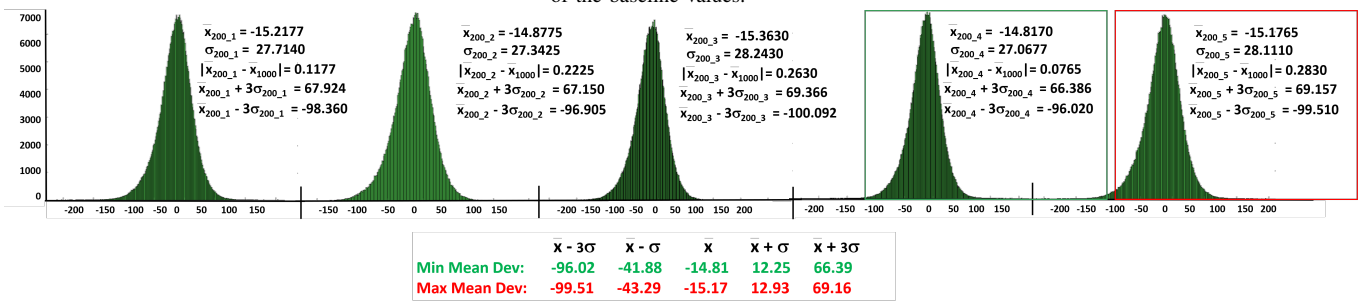
(d) Gaussian distribution, mean and standard deviation for 10x100 input vectors and also showing plots with the maximum (in Red box) and minimum (in Green box) mean deviation of 3σ values of *conv1* output for the 10x100 MNIST images when compared with baseline. It can be seen that even the maximum 3σ deviation, which helps this technique in defining RoVs (see Section IV), is within 2.50% of the baseline values.

Figure 7: Comparison of mean, standard deviation, Gaussian distribution and 3σ values of different sizes of datasets input images for LeNet CNN (CNN for MNIST dataset). These plots validate the hypothesis that with reduced dataset from 1000 input vectors to 10x 100 input vectors, each individual plot show similar Gaussian distributions with the baseline. The minimum and maximum mean deviations also fall around the same range

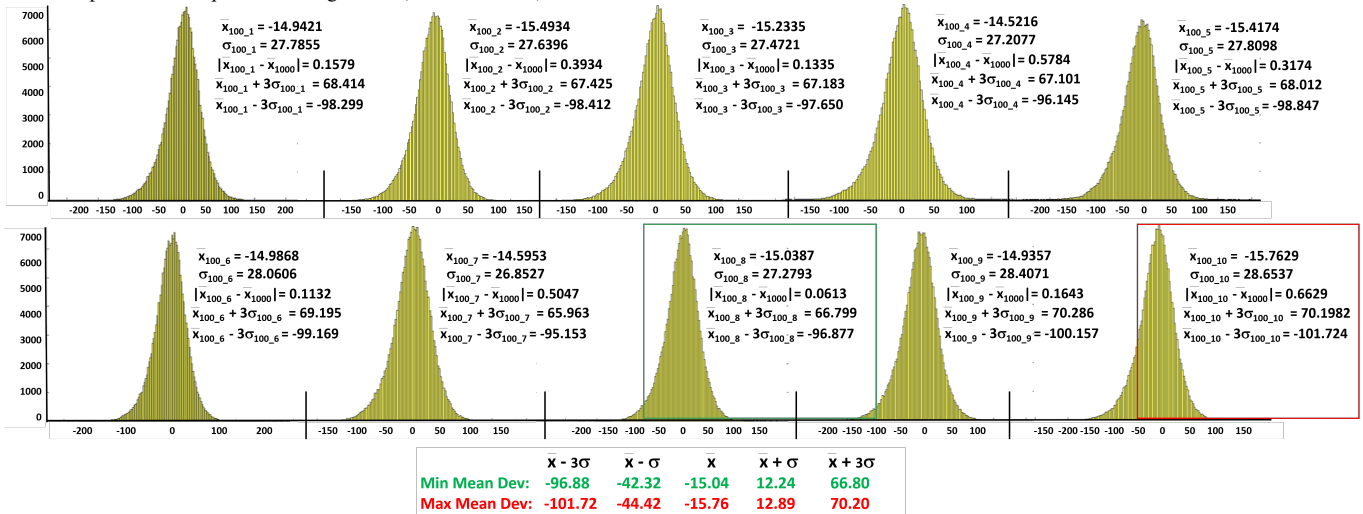


(a) Gaussian distribution, mean, standard deviation and 3σ values of conv1 output in response to 1000 input Cifar10 images (Baseline)

(b) Gaussian distribution, mean and standard deviation for 2x500 input vectors and also showing the maximum (in Red box) and minimum (in Green box) mean deviation of 3σ values of conv1 output for 2x500 Cifar10 images when compared with baseline. It can be seen that even the maximum 3σ deviation, which helps this technique in defining RoVs (see Section IV), is within 0.14% of the baseline values.



(c) Gaussian distribution, mean and standard deviation for 5x200 input vectors and also showing the maximum (in Red box) and minimum (in Green box) Mean deviation of 3σ values of conv1 output for 5x200 Cifar10 images when compared with baseline. It can be seen that even the maximum 3σ deviation, which helps this technique in defining RoVs (see Section IV), is within 2.36% of the baseline values.



(d) Gaussian distribution, mean and standard deviation and the maximum (in Red box) and minimum (in Green box) mean deviation of 3σ values for 10x100 input vectors Cifar10 images It can be seen that even the maximum 3σ deviation, which helps this technique in defining RoVs (see Section IV), is within 3.59% of the baseline values.

Figure 8: Comparison of mean, standard deviation, Gaussian distribution and 3σ values of different sizes of datasets input images for LeNet-3D CNN (CNN for Cifar10 dataset). These plots also validate that with reduced dataset from 1000 input vectors to 10x 100 input vectors, each individual plot show similar Gaussian distributions with the baseline. The minimum and maximum mean deviations also fall around the same range

$$I \sim \mathcal{N}(\mu, \sigma^2) \quad (4)$$

where μ and σ^2 represent the mean and variance of the distributions respectively.

Therefore, convolution operation between these weights (W) and input images or vectors (I) results in feature maps (F) that also follow Gaussian distribution according to Cramer's theorem [34].

$$I \circledast W = F \sim \mathcal{N}(\mu, \sigma^2) \quad (5)$$

Equation 5 is a corollary of Cramer's theorem [34].

B. METHODOLOGY OVERVIEW

Validation Dataset Sample Space

For the offline pre-processing phase, to obtain stealthy TBCs we require FM-Dataset. Figs 7 and 8 show a systematic approach employed in obtaining statistical attributes from a limited FM-Dataset made available to the 3PIP designer. This systematic approach involves the analysis of different dataset sizes in terms of the relationship between their feature maps and their statistical distribution. From the analysis, we obtain stealthy TBCs inserted in the hardware design to serve as the trigger. Fig. 3 shows these CNN models (LeNet and LeNet-3D) used for the classification of MNIST and Cifar10 datasets, respectively. LeNet CNN consist of 7 layers from convolution layer (*conv1*) to fully connected layer (*ip1*) excluding the classification layer (*ip2*) used for the prediction of MNIST datasets. LeNet-3D CNN is similar to LeNet CNN for classification of Cifar10 dataset, with the exception that the input image is RGB instead of gray scale. Gaussian distribution plot of the aggregated output feature maps of the CNN layers can be exploited for the FeSHI hardware attack. Figs. 7 and 8 show output feature maps of the *conv1* layer of LeNet and LeNet-3D CNN models for the MNIST and Cifar10 datasets respectively. MNIST dataset consists of 60,000 training images and 10,000 testing images [35]. We consider 10% of the testing images (1000 input vectors) as the baseline dataset. In order to find out minimal sample space to serve as the size of the FM-Dataset, that can provide the attacker with a good estimate of the statistical properties, the baseline input vectors is divided into different subsets. The respective statistical properties (mean and standard deviation) of the different subsets (the 1000 input vectors are randomly divided into different buckets of 2×500 , 5×200 , 10×100) of the 1000 input vectors (FM-Dataset) and compared with the properties of the baseline input vectors.

The approach shown in Figs. 7 and 8 provides an avenue of finding appropriate RoVs from seen data (FM-Dataset) that can be utilized as TBC during the inference phase applied for real-time classification on unseen data. The 3σ values of the subset buckets of the dataset showing the minimum and maximum mean deviations from the baseline of all the reduced datasets are compared with the baseline dataset. The RoVs are chosen from values that lie beyond the -3σ values on either side of the mean of

the Gaussian distribution. From the Gaussian distribution plots in Figs. 7, the 3σ regions of the plots with minimum mean deviation (across the 2×500 , 5×200 and 10×100 test vectors for LeNet) show highest percentage differences of 4.50%, 1.40%, and 2.50% respectively for the 3σ values in comparison with the baseline plot. From Fig. 8, the plots with maximum mean deviation (across the 2×500 , 5×200 and 10×100 test vectors for LeNet-3D) show highest percentage differences of 0.14%, 2.36%, and 3.59% respectively for the 3σ values in comparison with the baseline plots. Our results stated above validates our Hypothesis 1 which stipulates that we can estimate the statistical properties of a baseline dataset from a limited FM-Dataset. This is used to successfully obtain stealthy TBCs and design dynamic triggers discussed in Section IV-B.

The FeSHI methodology is divided into 2 stages namely: offline pre-processing stage and the run-time stage. An overview of the proposed Offline pre-processing stage is shown in Fig. 10. This stage provides a means of selecting one or more stealthy TBCs to serve as trigger(s) for the attack. These trigger(s) can be targeted at one or more layers depending on the choice of the adversary. This is further elaborated on in Section IV. The runtime operation discusses the resulting effect once the hardware Trojan is triggered, which is elaborated in Section V.

IV. OFFLINE PRE-PROCESSING: TBC TO DESIGN TRIGGERS

During the verification stage using the FM-Dataset, the adversary keeps track of the output feature maps of the CNN layers available as shown in Fig. 10. As discussed in Section III, due to the standard weight initialization approaches and innate random nature of incoming features, the computation results in an output feature map that follows Gaussian distribution. With this understanding, the attacker can obtain a particular RoVs (subsequently called Triggering Boundary Condition (TBC)) that lies beyond the $\pm 3\sigma$ values of the Gaussian distribution (as shown in line 7 of Algorithm 1 and explained in further detail in Sections IV-A and IV-B). The TBCs occur infrequently as seen in Fig. 10 and represent less than 1% of the total output feature map values across the FM-Dataset.

To validate that the output feature maps of CNN layers follow a Gaussian distribution, we analyzed them by plotting a histogram of their aggregated numerical values, as illustrated in Fig. 9. The histogram plots of the aggregated feature maps of each individual layer (from *conv1* to *ip1* layers) of LeNet CNN in response to 100 uniformly distributed images (serving as the FM-Dataset) are obtained and plotted in Fig. 9. The output feature maps, as expected, is having close conformity to Gaussian distribution from where an attacker can obtain the rare TBCs (e.g. for the case of *conv1* the value can be greater 450.2962 or less than -440.8916 , as indicated by the red arrows). These boundary conditions are obtained and used to design two types of attacks namely: Static attack, and dynamic attack.

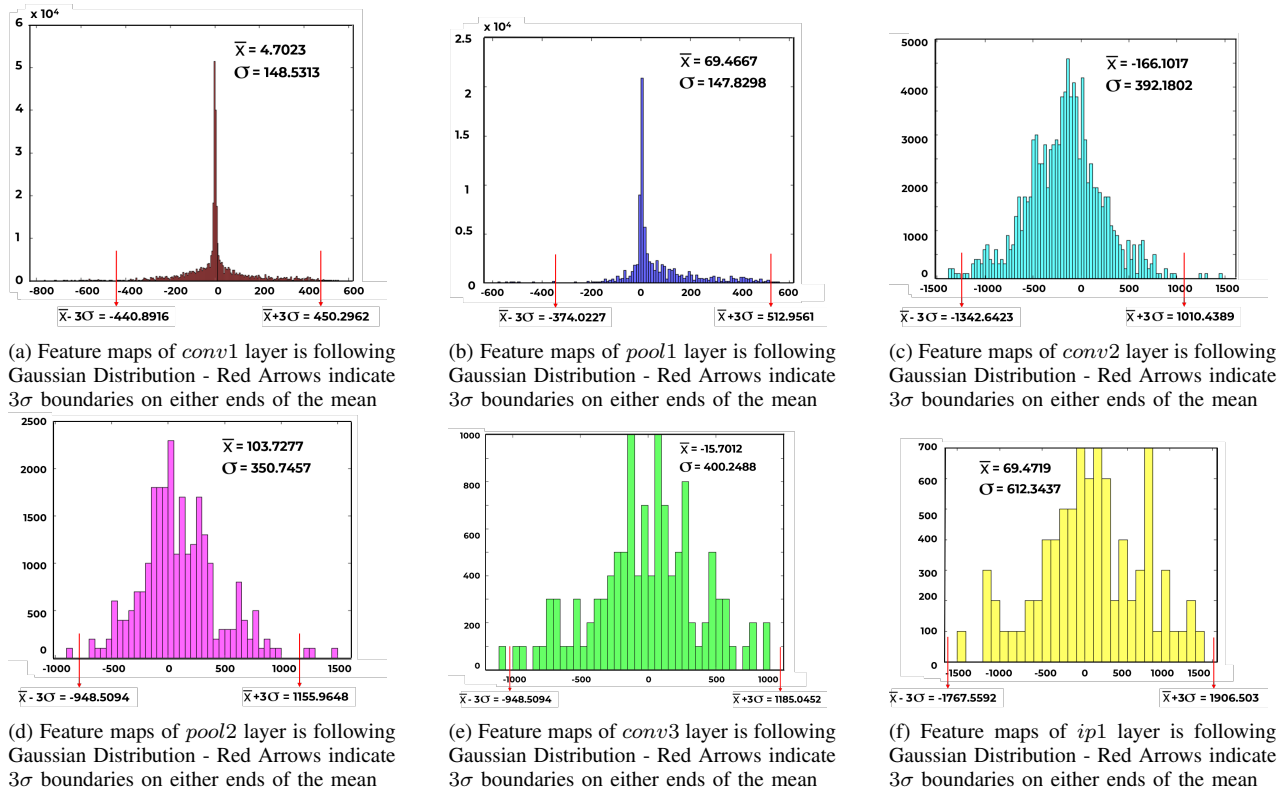


Figure 9: This set of simulation indicates that output feature maps of each CNN layer, in response to minimal input data (100 images), shows close conformity to Gaussian Distribution for LeNet CNN

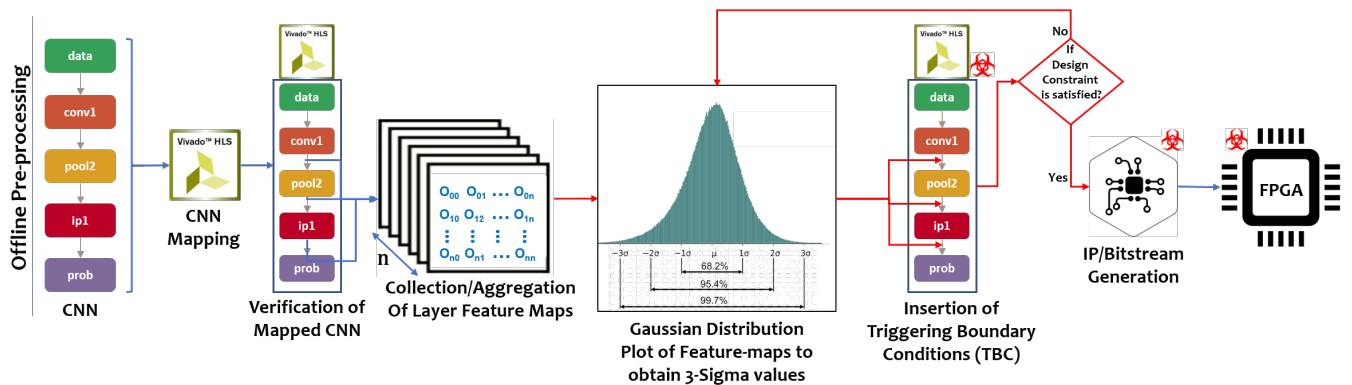


Figure 10: Proposed FeSHI methodology offline overview: The offline processing of the hardware Trojan showing the 3σ analysis, extraction of the triggering boundary conditions (TBC) and insertion of the hardware Trojan

These are further explained next.

A. STATIC ATTACK

In this attack, the attacker aggregates the feature maps generated in response to the FM-Dataset (as depicted in line 4 of Algorithm 1). The Gaussian distribution of the aggregated feature map is plotted to observe the 3σ values. One of the RoVs (as shown in line 6 – 9 of Algorithm 1) that lie beyond the 3σ values is selected and inserted into the hardware design to serve as the TBC for the attack to the targeted CNN layer available to the attacker as shown in Fig. 11. For the proposed design, the attack is evaluated

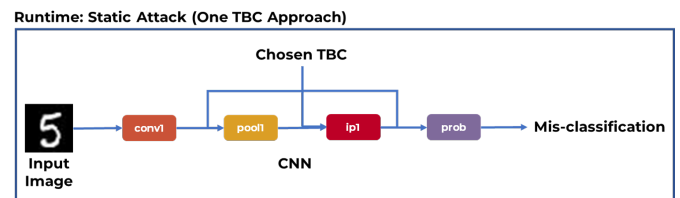


Figure 11: Static Attack Design showing the insertion of TBC trigger to the layer of the CNN available to the attacker

based on the Stealthiness (additional hardware overhead (BRAM, DSP, flip-flops (FFs), look-up tables (LUTs),

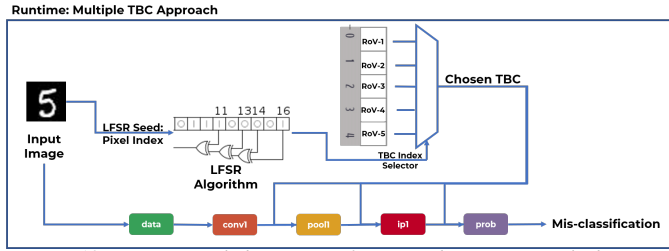


Figure 12: Conceptual depiction of FeSHI dynamic attack design showing the use of LFSR algorithm to implement different TBC trigger for different image instances- This may randomly choose one of the five RoV as a TBC, hence it creates another layer of illusion for such attacks to be detected using conventional test vector techniques.

Latency) and effectiveness (the rate of triggering) of the attack. Lines 9 – 18 of Algorithm 1 evaluates the selected TBC in terms of the degree of occurrence of the trigger (effectiveness) by testing it on the feature map of the targeted CNN layer using the FM-Dataset (seen data). If the amount of triggering satisfies some preset number set as the threshold amount of trigger occurrence, as seen in line 15 of Algorithm 1, then this RoV is set as the TBC. In this work, to achieve a maximum of 10% triggering probability, the threshold is set to 25 (number of occurrences). If the threshold condition is not satisfied then another RoV that lies beyond the 3σ values will be chosen and testing the threshold condition will be repeated. The threshold can be changed based on design choice in design time.

To achieve a resource-friendly design trade-off between resource usage and the number of possible triggers (that will lead to reduced accuracy), we provided three different variants of this attack which are discussed in Section IV-C (Lines 20 - 26 in Algorithm 1).

B. DYNAMIC ATTACK

In a situation where the defender tries to come up with test-vectors to detect hardware attacks due to such rarely occurring events, we propose a dynamic version of the FeSHI attack that changes its RoVs to boost stealthiness during runtime.

In this attack, after collection and aggregation of the feature maps, multiple set of RoVs that lie beyond the 3σ values of the Gaussian distribution of the aggregated feature maps are inserted as TBCs (depicted in lines 3 – 9 of Algorithm 2) in the hardware design in the form of an array (TBC array) as depicted in Fig. 12. In this work, an image cycle refers to every time an input image or feature map is passed as input for classification during runtime. From Fig. 12 during runtime, in an image cycle, the value present in a pre-selected index of an input image is normalized and serves as a seed to the LFSR (Linear Feedback Shift Registers) algorithm. LFSR algorithms are used for generating non-sequential sets of numbers in a time-efficient way by making use of right-shift and XOR operations [36].

The LFSR used in this work is a 6th-degree polynomial ($q^6 + q + 1$). In this work, the output of the LFSR algorithm is random integers between 0 – 4 in order to satisfy the selection of one of the 5 RoVs selected and inserted in the hardware design. The LFSR algorithm generates a TBC index selector (designated as *selector* in Algorithm 2) that lies within the length of the TBC array which serves as the select bit to the TBC array (array of multiple RoVs) multiplexer (as shown in Line 12 of Algorithm 2). Based on the TBC index selector, one of the RoVs in the TBC array is selected and inserted into the CNN layer to be attacked. This is depicted in Lines 11 - 16 of Algorithm 2. Here, 5 sets of RoVs are selected for the TBC array in order to increase randomness, improve stealthiness, and also incur minimum additional resources. The LFSR algorithm is used to randomly generate values from 0 to 4 serving as the TBC array index selector. The RoVs in TBC array corresponding to the index selected serve as the TBC trigger in the current image cycle. Lines 11 – 19 of Algorithm 2 evaluates the stealthiness of the LFSR algorithm and the selected RoVs serving as the TBC array. If the effectiveness satisfies the triggering threshold, the RoVs are selected. Lines 22 – 28 of Algorithm 2 shows the selection of appropriate attack variation approach in terms of resource utilization and attack variation in terms of layer-wise, channel-wise, or index-wise approach, this is discussed in the next subsection.

C. ATTACK TRIGGER VARIATIONS

Both static and dynamic attacks are implemented in three different variations of trigger design. These different variations of triggers show different design trade-offs between stealthiness, resources, and latency. Algorithms 1 and 2 consider these trade-offs and can provide a more resource-friendly solution for a given context (line 20 in Algorithm 1, and line 22 in Algorithm 2).

1) Layer-wise Trigger Design: Low Stealth/High Resource

In this trigger design, all the elements across all channels of the targeted CNN layer output feature map of interest are compared against the embedded TBC as shown in Fig. 13. If one or more of the values of the feature maps fall within the TBC, the payload gets activated. The probability of trigger getting activated is highest at the expense of high resources, see Table 2 for comparison.

2) Channel-wise Trigger Design: Medium Stealth/Medium Resource

In this case, all the elements of a channel of the targeted CNN layer output feature maps are compared against the predefined TBC as depicted in Fig. 13. If one or more elements in the channel satisfy the TBC, the payload gets activated. As shown in Table 2, it uses lesser resources than layer-wise trigger but consequently, the probability of getting triggered is also lesser.

Table 2: Chart comparing all of FeSHI attack variations in terms of Resources, Latency and Triggering Probability

Attack Variation	Resources	Latency (clock-cycles)	Triggering Probability
Layer-wise	Highest (This approach requires most resources to compare all the elements of the feature map to the TBC)	Highest (This approach requires the highest time because it compares all the elements of the feature maps to the TBC)	Highest (This compares all the elements of the feature map to the TBC)
Channel-wise	Medium (Requires fewer resources to compare only a channel of the feature map to the TBC)	Medium (Requires lower time to compare a channel of the feature maps to the TBC)	Medium (Only compares a channel of the feature maps to the TBC)
Index-wise	Lowest (Requires low additional resources to compare one value of the feature map to the TBC)	Lowest (Requires least time to compare one value of the feature map to the TBC)	Lowest (Only compares one value of the feature map to the TBC)

Offline Preprocessing

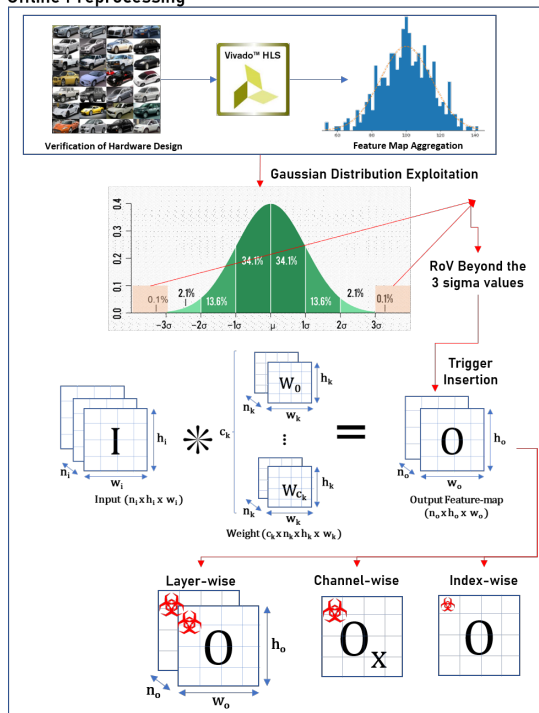


Figure 13: FeSHI offline trigger variation showing the insertion of 3σ values in either the layer (all of the channels of the feature map are compared to the selected TBC(s)) or channel (any one channel (x) of the feature map is compared to the selected TBC(s)) or a particular index (just one value of the feature map are compared to the selected TBC(s)) of the feature maps

3) Index-wise Trigger Design: High Stealth/Low Resource

In this case, only an index in the targeted CNN layer output feature map is monitored and compared with the predefined TBC as shown in Fig. 13. If the value of the chosen index satisfies the TBC, the payload gets activated. This requires the least resources and consumes the least latency, but also triggering probability is also the least among all the variants of this attack as stated in Table 2.

Algorithm 1 Offline pre-processing: Static Attack where: DC: Design Constraints LW: Layer-wise CW: Channel-wise

Require: Mapping of the CNN in HLS (C++).

Require: Verification of design

- 1: Identify targeted layer L
- 2: $trig = 0$ (number of triggers)
- 3: **for** image (X_i) \in FM-Dataset **do**
- 4: Collect $AF = \{O_1, O_2, \dots, O_{n_o}\}$
Where: $O_i, \dots, O_{n_o} \in O$ (Values in the feature maps)
 n_o is the maximum amount of channels in the feature maps
 AF represent aggregated feature maps
- 5: **end for**
- 6: Obtain values beyond 3σ values in AF .
- 7: Collect low occurring RoV $[a, b] \in AF$
where: a represent the lower limit of the selected RoV
 b represent the upper limit of the selected RoV
- 8: Insert $[a, b]$ in Hardware design
- 9: Test $[a, b]$
- 10: **for** image (X_i) \in FM-Dataset **do**
- 11: **if** ($\{O_i, \dots, O_z\} \in [a, b]$) **then**
- 12: $trig+ = 1$
- 13: **end if**
- 14: **end for**
- 15: **if** $trig \leq threshold$ **then**
- 16: Insert $[a, b]$ as TBC
- 17: **else**
- 18: Repeat steps 3 to 16
- 19: **end if**
where: $threshold$ represent the desired maximum amount of times a number in the feature map of a layer falls in the seleted RoVs in response to the FM-Dataset
- 20: **if** TBC \in DC as LW trigger **then**
- 21: Insert TBC as LW trigger
- 22: **else if** TBC \in DC as CW trigger **then**
- 23: Insert TBC as CW trigger
- 24: **else**
- 25: Insert as index-wise trigger
- 26: **end if**

Algorithm 2 Offline pre-processing: Dynamic Attack where: DC: Design Constraints LW: Layer-wise CW: Channel-wise

Require: Mapping of the CNN in HLS (C++).

Require: Verification of design

- 1: Identify targeted layer L
- 2: $trig = 0$
- 3: **for** image $(X_i) \in$ FM-Dataset **do**
- 4: Collect $AF = \{O_1, O_2, \dots, O_{no}\}$
- 5: **end for**
- 6: Obtain values beyond 3σ values in AF .
- 7: Collect 5 low occurring RoVs $\{[A_0, B_0], [A_1, B_1], \dots, [A_z, B_z]\} \in AF$ Where: $A_0 - A_z$ represent the upper limits of the selected ROVs
 $B_0 - B_z$ represent the lower limits of the selected ROVs
 z is the maximum amount of RoVs collected
- 8: Insert $\{[A_0, B_0], [A_1, B_1], \dots, [A_z, B_z]\}$ as TBCs in hardware design
- 9: Test $\{[A_0, B_0], [A_1, B_1], \dots, [A_z, B_z]\}$
- 10: Insert $LFSR$ algorithm in hardware design
- 11: **for** image $(X_i) \in$ FM-Dataset **do**
- 12: $selector = LFSR(X_i[indx])$
- 13: **if** $\{O_i, \dots, O_{no}\} \in \{[A_0, B_0], [A_1, B_1], \dots, [A_z, B_z]\}$ **then**
- 14: $trig+ = 1$
- 15: **end if**
- 16: **end for**
- 17: **if** $trig \leq threshold$ **then**
- 18: Insert $\{[A_0, B_0], [A_1, B_1], \dots, [A_z, B_z]\}$ as TBC
- 19: **else**
- 20: Repeat steps 3 to 18
- 21: **end if**
- 22: **if** TBC \in DC as LW trigger **then**
- 23: Insert TBC as LW trigger
- 24: **else if** TBC \in DC as CW trigger **then**
- 25: Insert TBC as CW trigger
- 26: **else**
- 27: Insert index-wise trigger
- 28: **end if**

V. RUNTIME OPERATION: DESIGN OF THE PAYLOAD OF THE HARDWARE ATTACK

Algorithm 3 Payload Operation

Require: CNN Deployment

- 1: **for** each image cycle (X_i) **do**
- 2: **if** $(\{O_i, \dots, O_z\} \in [a, b])$ (when triggered) **then**
- 3: **for** $i \rightarrow y$ (where $y < z$) **do**
- 4: $O_i = 0$
- 5: **end for**
- 6: **end if**
- 7: **end for**
 y represent number of values in the feature maps rounded down to zero
 z represents total number of values in the feature maps of a layer

In this work, the payload of the hardware attack is designed to change the values of a feature map of a targeted CNN layer. The proposed payload randomly rounds a number of elements across all channels of the targeted feature maps to zero as seen in Lines 2 – 6 in Algorithm 3 depending on the amount of accuracy loss desired. This is depicted in Fig. 14. Since in our threat model the attacker may not know the exact location of the CNN layer in the overall CNN architecture where they are conducting the attack. Therefore, we demonstrated an analysis on the example network to understand how difficult it is for the attacker to conduct the attack. To achieve this understanding, an empirical study is carried out on LeNet (for MNIST dataset - LeNet architecture is shown in Fig. 3) to determine the minimum number of values (y shown in Line 3 of Algorithm 3) of the output feature map that needs to be rounded to zero across all the channels of the targeted CNN layer to guarantee misclassification at the final output. After this determination, the minimum number of values for the output feature maps of interest is inserted into the hardware design. The payload can be inserted into one or more CNN layer(s). Table 3 shows results of the empirical study of the number of values in a feature map of a layer to be rounded to zero to cause decrease in accuracy of the mapped CNN (10%, 50%, 90% accuracy decrease respectively) and their corresponding resource utilization for $conv1$ and $conv2$ of LeNet CNN. This empirical study is carried out on only two layers because our goal is just to validate the effect of the proposed payload on high resource requirement layers (in this case $conv1$ and $conv2$ layers). For the $conv1$ layer, to achieve 10%, 50% or 90% accuracy loss, 29%, 67% or 92% of the values of the feature maps required to be rounded down to zero respectively.

For the $conv2$ layer, to achieve 10%, 50% or 90% accuracy loss, 38%, 63% or 88% of the values of the feature maps required to be rounded down to zero respectively. The result shows that to achieve high accuracy loss, more feature map locations are needed to be rounded to zero. The hardware resources required to achieve 90% accuracy loss for

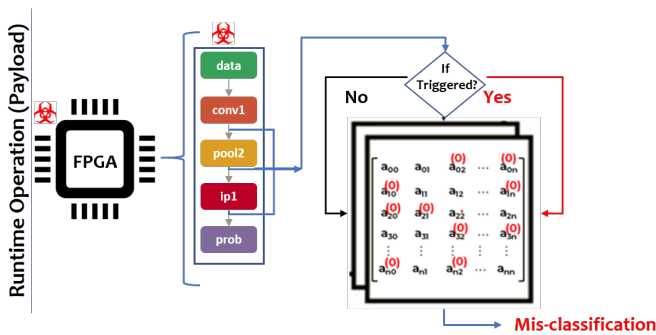


Figure 14: Proposed FeSHI methodology runtime overview: The runtime operation of the hardware Trojan showing the payload. The conversion of feature maps to achieve misclassification

Table 3: Payload’s Empirical Analysis to find the Relationship between the Amount of values rounded down to zero for a given feature map and Loss of Accuracy. This is carried out on LeNet CNN using Vivado HLS 2018.3 for PYNQ FPGA Board (ZYNQ 7020).

Layer	feature map	No.	Accuracy loss											
			10%				50%				90%			
			#	FF	LUT	Lat.	#	FF	LUT	Lat.	#	FF	LUT	Lat.
conv1	6 x 24 x 24	3456	1008	35370	40279	610688	2304	35766	40512	610796	3168	35761	40536	610868
conv2	16 x 8 x 8	1024	384	35740	40776	601046	640	35742	40779	601058	896	35748	40802	601066

No. represent the total number of values in feature maps

represents the total number of values rounded to zero

Lat. represent latency in terms of clock-cycles

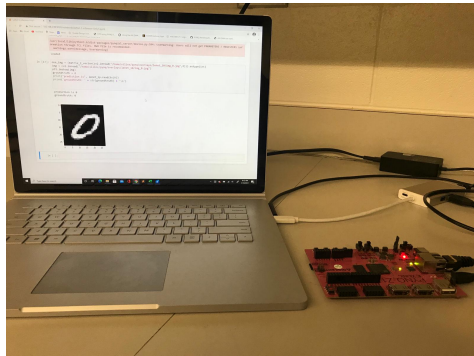


Figure 15: Experiment Setup showing realtime classification of MNIST dataset on PYNQ FPGA using python overlay

both *conv1* and *conv2* layers show a maximum percentage difference of 14% from the original implementation using this payload.

Table 3 shows that the number of resources needed (in terms of flip-flops (FF), lookup tables (LUT), and latency (Lat)) is proportional to the number of values needed to be rounded down to zero. This helps the attacker evaluate the effectiveness of the payload and come up with a stealthiness-effectiveness compromise.

VI. EXPERIMENTAL SETUP FOR HARDWARE DEPLOYMENT, RESULTS, AND DISCUSSION

The hardware design of the CNN IP is designed using Xilinx’s Vivado and Vivado HLS 2018.3 and to generate an IP for resource-constrained devices. Vivado 2018.3 is used to integrate the generated IP with AXI-interconnects and ZYNQ processor (FPGA ZCU 7020 with clock frequency 100MHz) and implemented on PYNQ FPGA board. The attack is carried out on LeNet CNN trained on MNIST dataset and LeNet-3D CNN trained on Cifar10 datasets as shown in Fig. 3, respectively. The experimental setup is shown in Fig. 15

In this work, we propose 6 different scenarios (Scenario 1 (*Sn1*) - Scenario 6 (*Sn6*)) of both static and dynamic attacks, where each layer (from *conv1* to *ip1*) is infected with the attack. Table 4 shows results of the static and dynamic attack on the LeNet CNN model. For both static and dynamic attacks across all the attack scenarios (*Sn1* – *Sn6*) and variations (layer/channel/index), the BRAM and DSP utilization remain the same (0% difference) when compared

to the original implementation. In this work, we have chosen to round down 90% of the feature map values to zero as a worst-case payload for LeNet and LeNet-3D models with results based on the additional resources and latency overhead shown in Tables 4 and 5, respectively. **From Table 4, for the static attack**, LUT utilization across *Sn1* – *Sn6* show a maximum of 0.064% percentage difference compared to the original, which is in the case of *Sn2* channel attack. FFs across *Sn1* – *Sn6* shows a maximum of 0.0189% percentage difference compared to the original, which is in the case of *Sn1* channel attack and *Sn3* layer attack. Across *Sn1* – *Sn6*, the latency shows a maximum percentage difference of 0.067% compared to the original, which is in the case of *Sn1* layer attack. Both the dynamic and total power usage shows a maximum of 0.005% percentage difference when compared to the original. **In the case of the dynamic attack**, across all the attack scenarios, *Sn1* – *Sn6*, LUT utilization shows a maximum of 0.056% percentage difference, the FFs usage shows a maximum of 0.029%, the latency shows the highest percentage difference of 0.066%, the dynamic power shows a maximum percentage difference of 0.004% and the total power usage shows a maximum percentage difference of 0.005% when respectively compared to the original (shown in the first row of Table 4). Hence, from these attack scenarios, FeSHI static and dynamic attacks across the LeNet CNN layers are stealthy due to the negligible amount of additional hardware resources required to carry out the attack.

Table 5 shows results of the static and dynamic attacks on the LeNet-3D CNN model. The result shows that BRAM and DSP usage remains the same both static and dynamic attacks across all the attack scenarios and stages except for one scenario of dynamic attack (*conv1channel*) which shows 0.38% percentage difference when compared to the original. Also from Table 5, for the static attack, LUT utilization across *Sn1* – *Sn6* shows a maximum percentage difference of 0.043% compared to the original, which is in the case of *Sn3* channel attack. FFs across *Sn1* – *Sn6* show a maximum percentage difference of 0.011% when compared to the original, which is in the case of *Sn2* index attack. Across *Sn1* – *Sn6*, the latency shows a maximum percentage difference of 0.064% compared to the original, which is in the case of *Sn1* layer attack. Dynamic power usage shows a maximum percentage difference of 0.026%

Table 4: Hardware resource utilization comparison for both static and dynamic attack on LeNet CNN for MNIST dataset. The BRAM and DSP resource utilization shows 0% percentage difference across all attack scenarios for both static and dynamic attack respectively

Network	Scenario	Stage	#No	LUTs	% diff	FFs	% diff	Latency clock-cycles	% diff	Dynamic Power	% diff	Total Power	% diff
LeNet Static Attack	Original	-	-	39387	-	35703	-	596086	-	1.505	-	1.648	-
	S_{n1} : conv1attack	Layer	3456	41668	0.0547	36385	0.0187	638702	0.067	1.513	0.005	1.652	0.002
		Channel	576	41719	0.0559	36390	0.0189	615712	0.032	1.511	0.004	1.655	0.004
		Index	1	41465	0.0501	36331	0.0173	610626	0.024	1.508	0.002	1.651	0.002
	S_{n2} : pool1attack	Layer	864	41628	0.0538	36367	0.0183	602996	0.011	1.512	0.005	1.656	0.005
		Channel	144	41673	0.0549	36371	0.0184	597265	0.002	1.509	0.003	1.653	0.003
		Index	1	41423	0.0492	36317	0.0169	596088	0.000	1.513	0.005	1.656	0.005
	S_{n3} : conv2attack	Layer	1024	42043	0.0632	36389	0.0189	609243	0.022	1.501	0.003	1.652	0.002
		Channel	64	42078	0.0640	36388	0.0188	601577	0.009	1.511	0.004	1.653	0.003
		Index	1	41839	0.0586	36337	0.0174	601055	0.008	1.504	0.001	1.655	0.004
	S_{n4} : pool2attack	Layer	256	41582	0.0528	36325	0.0171	595634	0.001	1.51	0.003	1.651	0.002
		Channel	16	41613	0.0535	36365	0.0182	595491	0.001	1.508	0.002	1.654	0.004
		Index	1	41473	0.0503	36331	0.0173	595392	0.001	1.512	0.005	1.655	0.004
	S_{n5} : conv3attack	Layer/Channel	84	41725	0.0560	36382	0.0187	594162	0.003	1.507	0.001	1.652	0.002
		Index	1	41632	0.0539	36359	0.0180	596017	0.000	1.513	0.005	1.651	0.002
	S_{n6} : ip1attack	Layer/Channel	100	41452	0.0498	36339	0.0175	595874	0.000	1.502	0.002	1.65	0.001
		Index	1	41639	0.0541	36342	0.0176	595243	0.001	1.503	0.001	1.653	0.003
	LeNet Dynamic Attack	S_{n1} : conv1attack	Layer	3456	41668	0.055	36384	0.019	638301	0.066	1.513	0.005	1.652
Channel			576	41719	0.056	36392	0.019	615712	0.032	1.508	0.002	1.653	0.003
Index			1	41465	0.050	36352	0.018	610626	0.024	1.509	0.003	1.652	0.002
S_{n2} : pool1attack		Layer	864	41628	0.054	36328	0.017	602996	0.011	1.512	0.005	1.651	0.002
		Channel	144	41673	0.055	36371	0.018	597265	0.002	1.511	0.004	1.653	0.003
		Index	1	41423	0.049	36317	0.017	596088	0.000	1.509	0.003	1.655	0.004
S_{n3} : conv2attack		Layer	1024	41572	0.053	36320	0.017	596032	0.000	1.508	0.002	1.653	0.003
		Channel	64	41376	0.048	36383	0.019	569342	0.047	1.511	0.004	1.652	0.002
		Index	1	41427	0.049	36714	0.028	595450	0.001	1.512	0.005	1.651	0.002
S_{n4} : pool2attack		Layer	256	41698	0.055	36751	0.029	595903	0.000	1.511	0.004	1.655	0.004
		Channel	16	41465	0.050	36724	0.028	595821	0.000	1.513	0.005	1.652	0.002
		Index	1	41512	0.051	36656	0.026	594965	0.002	1.508	0.002	1.651	0.002
S_{n5} : conv3attack		Layer/Channel	84	41565	0.052	36718	0.028	596392	0.001	1.511	0.004	1.655	0.004
		Index	1	41354	0.048	36675	0.027	595197	0.001	1.512	0.005	1.652	0.002
S_{n6} : ip1attack		Layer/Channel	100	41562	0.052	36718	0.028	596033	0.000	1.509	0.003	1.655	0.004
		Index	1	41356	0.048	36653	0.026	595197	0.001	1.513	0.005	1.651	0.002

#No. represent the total number of values in feature maps

when compared to the original, which occurs in the case of S_{n1} channel attack. While total power usage shows a maximum percentage difference of 0.024% when compared to the original, which occurs in the case of S_{n1} layer and channel attack.

In the case of the dynamic attack for LeNet-3D, across all the attack scenarios, $S_{n1} - S_{n6}$, LUT utilization shows a maximum of 0.033% percentage difference in S_{n1} channel attack, the FFs usage shows a maximum of 0.002% in S_{n1} channel attack and S_{n1} layer and channel attack, the latency shows the highest percentage difference of 0.034% in the case of S_{n1} layer attack, the dynamic power shows a percentage difference of maximum of 0.026% in S_{n1} channel attack and the total power usage shows a maximum of 0.028% percentage difference in S_{n1} channel attack when compared respectively compared to the original. These results also confirm that the proposed FeSHI static and dynamic attacks across the LeNet-3D CNN layers are stealthy due to the negligible amount of additional hardware resources required to carry out the attack.

To demonstrate the randomness in the triggering of the proposed attack, various random input datasets are exam-

ined. In Figs. 16 and 17, we randomly select and provide five different datasets (200 images each) to LeNet and LeNet-3D CNNs, the static and dynamic attack variations are investigated from the layer-wise, channel-wise, and index-wise perspectives. For and LeNet CNN, considering S_{n1} the number of trigger occurrences varies randomly between 10 and 20 in the layer-wise triggering approach, 4 and 15 in the channel-wise triggering approach, 0 and 5 in the index-wise triggering approach. The same is true for other attack scenarios- making our attack random and stealthy. During design time, we experienced certain triggering probability on seen data (FM-Dataset).

VII. CONCLUSION AND FUTURE WORKS

In this paper, we propose a hardware Trojan attack that performs a statistical analysis on the layer-by-layer output of CNN models to obtain stealthy triggering conditions. This attack is a grey box attack that is carried out in the hardware implementation stage of CNN architecture. This attack is demonstrated on two CNN models used to perform classification on MNIST and Cifar-10 data sets. The Trojan proved to be stealthy and adds negligible hardware

Table 5: Hardware resource utilization comparison for both static and dynamic attack on LeNet-3D CNN for Cifar10 dataset. The BRAM and DSP resource utilization shows 0% percentage difference across all attack scenarios for both static and dynamic attack except for one scenario of dynamic attack (conv1 – channel) which shows 0.38 percentage difference

Network	Scenario	Stage	#No	LUTs	% diff	FFs	% diff	Latency clock-cycles	% diff	Dynamic Power	% diff	Total Power	% diff
LeNet-3D Static Attack	Original	-	-	56321	-	72818	-	1441914	-	1.710	-	1.872	-
	Sn1 : conv1attack	Layer	3456	58515	0.037	73521	0.010	1540794	0.064	1.754	0.025	1.918	0.024
		Channel	576	58557	0.038	73525	0.010	1483802	0.028	1.755	0.026	1.919	0.024
		Index	1	58325	0.034	73460	0.009	1477475	0.024	1.753	0.025	1.916	0.023
	Sn2 : pool1attack	Layer	864	58450	0.036	73488	0.009	1455635	0.009	1.727	0.010	1.889	0.009
		Channel	144	58492	0.037	73491	0.009	1443315	0.001	1.721	0.006	1.883	0.006
		Index	1	58739	0.041	73611	0.011	1441918	0.000	1.724	0.008	1.887	0.008
	Sn3 : conv2attack	Layer	1024	58804	0.042	73532	0.010	1467662	0.018	1.729	0.011	1.892	0.011
		Channel	64	58846	0.043	73534	0.010	1452482	0.007	1.736	0.015	1.899	0.014
		Index	1	58618	0.039	73472	0.009	1451661	0.007	1.715	0.003	1.877	0.003
	Sn4 : pool2attack	Layer	256	58744	0.041	73472	0.009	1445915	0.003	1.705	0.003	1.867	0.003
		Channel	16	58788	0.042	73473	0.009	1442125	0.000	1.725	0.009	1.887	0.008
		Index	1	58562	0.038	73416	0.008	1441914	0.000	1.706	0.002	1.867	0.003
	Sn5 : conv3attack	Layer/Channel	84	58124	0.031	73473	0.009	1442715	0.001	1.72	0.006	1.882	0.005
		Index	1	57955	0.028	73421	0.008	1441914	0.000	1.715	0.003	1.877	0.003
	Sn6 : ip1attack	Layer/Channel	100	58124	0.031	73452	0.009	1443116	0.001	1.731	0.012	1.893	0.011
		Index	1	58744	0.041	73472	0.009	1445915	0.003	1.705	0.003	1.867	0.003
	LeNet -3D Dynamic Attack	Sn1 : conv1attack	Layer	3456	56971	0.011	72922	0.001	1493154	0.034	1.752	0.024	1.916
Channel			576	54538	0.033	72666	0.002	1420401	0.015	1.666	0.026	1.821	0.028
Index			1	56789	0.008	72864	0.001	1477475	0.024	1.732	0.013	1.895	0.012
Sn2 : pool1attack		Layer	864	56963	0.011	72893	0.001	1445835	0.003	1.724	0.008	1.887	0.008
		Channel	144	57005	0.012	72896	0.001	1442335	0.000	1.727	0.010	1.889	0.009
		Index	1	56789	0.008	72841	0.000	1441916	0.000	1.723	0.008	1.886	0.007
Sn3 : conv2attack		Layer	1024	57260	0.016	72933	0.002	1455662	0.009	1.733	0.013	1.896	0.013
		Channel	64	57302	0.017	72935	0.002	1451882	0.007	1.724	0.008	1.886	0.007
		Index	1	57082	0.013	72877	0.001	1451661	0.007	1.724	0.008	1.886	0.007
Sn4 : pool2attack		Layer	256	57200	0.015	72873	0.001	1442915	0.001	1.701	0.005	1.862	0.005
		Channel	16	57244	0.016	72874	0.001	1441975	0.000	1.704	0.004	1.866	0.003
		Index	1	57026	0.012	72821	0.000	1441914	0.000	1.701	0.005	1.862	0.005
Sn5 : conv3attack		Layer/Channel	84	56580	0.005	72874	0.001	1442115	0.000	1.708	0.001	1.869	0.002
		Index	1	56413	0.002	72826	0.000	1441914	0.000	1.71	0.000	1.871	0.001
Sn6 : ip1attack		Layer/Channel	100	56321	0.000	72818	0.000	1441914	0.000	1.703	0.004	1.865	0.004
		Index	1	56321	0.000	72818	0.000	1441914	0.000	1.71	0.000	1.872	0.000

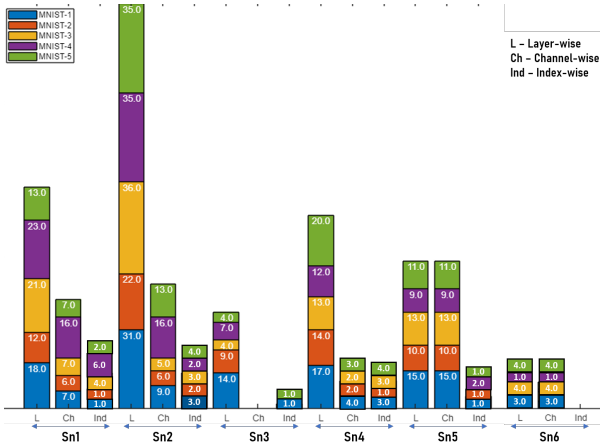
#No. represent the total number of values in feature maps

overhead.

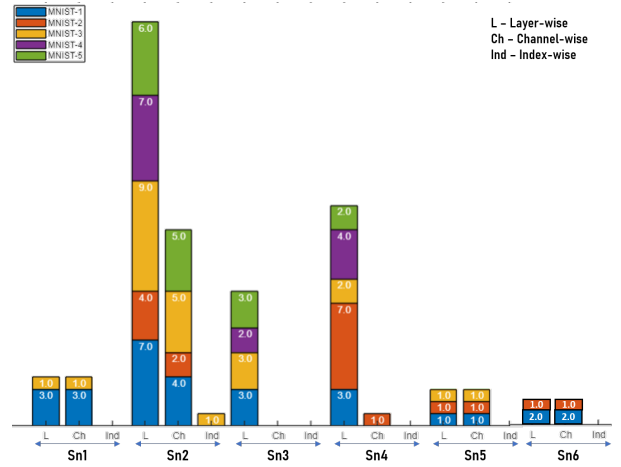
...

References

- [1] X. Zhang, Y. Wang, S. Lu, L. Liu, W. Shi et al., "Openai: An open framework for edge intelligence," in 2019 IEEE 39th International Conference on Distributed Computing Systems (ICDCS). IEEE, 2019, pp. 1840–1851.
- [2] B. Du, S. Azimi, C. De Sio, L. Bozzoli, and L. Sterpone, "On the reliability of convolutional neural network implementation on sram-based fpga," in 2019 IEEE International Symposium on Defect and Fault Tolerance in VLSI and Nanotechnology Systems (DFT). IEEE, 2019, pp. 1–6.
- [3] R. Ayachi, Y. Said, and A. B. Abdelali, "Optimizing Neural Networks for Efficient FPGA Implementation: A Survey," Archives of Computational Methods in Engineering, pp. 1–11, 2021.
- [4] N. Zhang, X. Wei, H. Chen, and W. Liu, "FPGA Implementation for CNN-based optical remote sensing object detection," Electronics, vol. 10, no. 3, p. 282, 2021.
- [5] Z. Mo, D. Luo, T. Wen, Y. Cheng, and X. Li, "FPGA Implementation for Odor Identification with Depthwise Separable Convolutional Neural Network," Sensors, vol. 21, no. 3, p. 832, 2021.
- [6] O. Iqbal, S. Siddiqui, J. Martin, S. Katoch, A. Spanias, D. Bliss, and S. Jayasuriya, "Design and FPGA Implementation Of An Adaptive Video Subsampling Algorithm For Energy-Efficient Single Object Tracking," in International Conference on Image Processing (ICIP). IEEE, 2020, pp. 3065–3069.
- [7] X. Xu and B. Liu, "Fclnn: a flexible framework for fast cnn prototyping on fpga with opencl and caffe," in 2018 International Conference on Field-Programmable Technology (FPT). IEEE, 2018, pp. 238–241.
- [8] X. Huang, E. Jones, S. Zhang, S. Xie, S. Furber, Y. Goulermas, E. Marsden, I. Baistow, S. Mitra, and A. Hamilton, "An FPGA Implementation of Convolutional Spiking Neural Networks for Radioisotope Identification," arXiv preprint arXiv:2102.12565, 2021.
- [9] Z. Liu, E. Ren, L. Luo, Q. Wei, X. Wu, X. Li, F. Qiao, X.-J. Liu, and H. Yang, "A 1.8 mw perception chip with near-sensor processing scheme for low-power aiot applications," in 2019 IEEE Computer Society Annual Symposium on VLSI (ISVLSI). IEEE, 2019, pp. 447–452.
- [10] T. A. Odetola and S. R. Hasan, "Sowaf: Shuffling of weights and feature maps: A novel hardware intrinsic attack (hia) on convolutional neural network (cnn)," 2021.
- [11] Y. Liu, S. Ma, Y. Aafer, W.-C. Lee, J. Zhai, W. Wang, and X. Zhang, "Trojaning attack on neural networks," in Network and Distributed System Security Symposium, NDSS. The Internet Society, 2018.
- [12] J. Clements and Y. Lao, "Hardware trojan attacks on neural networks," arXiv preprint arXiv:1806.05768, 2018.
- [13] —, "Hardware trojan design on neural networks," in 2019 IEEE International Symposium on Circuits and Systems (ISCAS). IEEE, 2019, pp. 1–5.
- [14] Y. Zhao, X. Hu, S. Li, J. Ye, L. Deng, Y. Ji, J. Xu, D. Wu, and Y. Xie, "Memory trojan attack on neural network accelerators," in 2019 Design, Automation & Test in Europe Conference & Exhibition (DATE). IEEE, 2019, pp. 1415–1420.
- [15] Z. Liu, J. Ye, X. Hu, H. Li, X. Li, and Y. Hu, "Sequence triggered

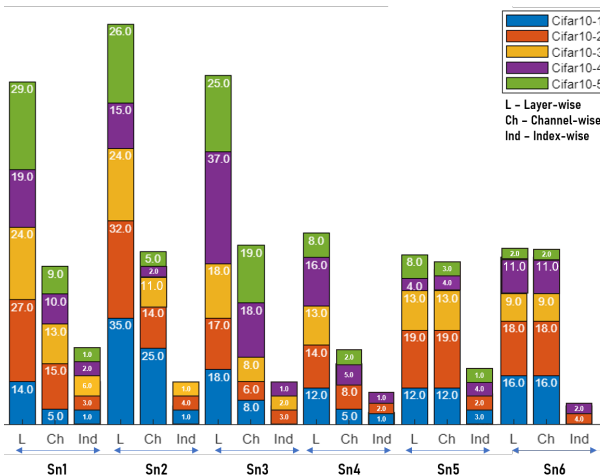


(a) Graph showing the random nature and low-triggering rate of the different static attack scenarios for the different variations (layer-wise, channel-wise and index-wise) on LeNet CNN

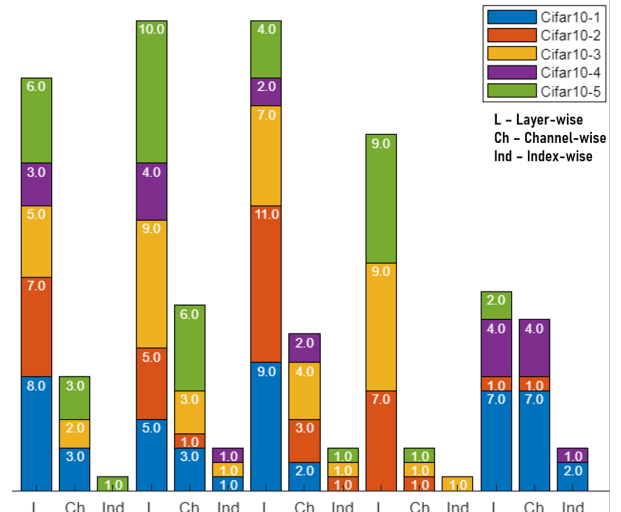


(b) Graph showing the random nature and low-triggering rate of the different dynamic attack scenarios for the different variations (layer-wise, channel-wise and index-wise) on LeNet CNN

Figure 16: Graph showing the random nature and low-triggering rate of the different attack scenarios for LeNet CNN on MNIST dataset



(a) Graph showing the random nature and low-triggering rate of the different static attack scenarios for the different variations (layer-wise, channel-wise and index-wise) on LeNet-3D CNN



(b) Graph showing the random nature and low-triggering rate of the different dynamic attack scenarios for the different variations (layer-wise, channel-wise and index-wise) on LeNet-3D CNN

Figure 17: Graph showing the random nature and low-triggering rate of the different attack scenarios for LeNet-3D CNN on Cifar10 dataset

hardware trojan in neural network accelerator,” in 2020 IEEE 38th VLSI Test Symposium (VTS). IEEE, 2020, pp. 1–6.

[16] M. Hailesellase, J. Nelson, F. Khalid, and S. R. Hasan, “Vaws: Vulnerability analysis of neural networks using weight sensitivity,” in 2019 IEEE 62nd International Midwest Symposium on Circuits and Systems (MWSCAS). IEEE, 2019, pp. 650–653.

[17] M. Zou, Y. Shi, C. Wang, F. Li, W. Song, and Y. Wang, “Potrojan: powerful neural-level trojan designs in deep learning models,” arXiv preprint arXiv:1802.03043, 2018.

[18] R. Hadidi, J. Cao, M. Woodward, M. S. Ryoo, and H. Kim, “Distributed perception by collaborative robots,” IEEE Robotics and Automation Letters, vol. 3, no. 4, pp. 3709–3716, 2018.

[19] D. Hu and B. Krishnamachari, “Fast and accurate streaming cnn inference via communication compression on the edge,” in 2020 IEEE/ACM Fifth International Conference on Internet-of-Things Design and Implementation (IoTDI). IEEE, 2020, pp. 157–163.

[20] J. Mao, X. Chen, K. W. Nixon, C. Krieger, and Y. Chen, “Modnn: Local

distributed mobile computing system for deep neural network,” in Design, Automation & Test in Europe Conference & Exhibition (DATE), 2017. IEEE, 2017, pp. 1396–1401.

[21] J. Mao, Z. Yang, W. Wen, C. Wu, L. Song, K. W. Nixon, X. Chen, H. Li, and Y. Chen, “Mednn: A distributed mobile system with enhanced partition and deployment for large-scale dnns,” in 2017 IEEE/ACM International Conference on Computer-Aided Design (ICCAD). IEEE, 2017, pp. 751–756.

[22] X. Zhang, H. Chen, and F. Koushanfar, “Tad: Trigger approximation based black-box trojan detection for ai,” arXiv preprint arXiv:2102.01815, 2021.

[23] Y. Gao, C. Xu, D. Wang, S. Chen, D. C. Ranasinghe, and S. Nepal, “Strip: A defence against trojan attacks on deep neural networks,” in Proceedings of the 35th Annual Computer Security Applications Conference, 2019, pp. 113–125.

[24] B. G. Doan, E. Abbasnejad, and D. C. Ranasinghe, “Februus: Input purification defense against trojan attacks on deep neural network systems,” in Annual Computer Security Applications Conference, 2020, pp. 897–912.

- [25] Y. Shen, M. Ferdman, and P. Milder, "Maximizing cnn accelerator efficiency through resource partitioning," in 2017 ACM/IEEE 44th Annual International Symposium on Computer Architecture (ISCA). IEEE, 2017, pp. 535–547.
- [26] L. Zeng, E. Li, Z. Zhou, and X. Chen, "Boomerang: On-demand cooperative deep neural network inference for edge intelligence on the industrial internet of things," IEEE Network, vol. 33, no. 5, pp. 96–103, 2019.
- [27] T. A. Odetola, K. M. Groves, and S. R. Hasan, "2i-3w: 2-level 3-way hardware-software co-verification for the mapping of deep learning architecture (dla) onto fpga boards," arXiv preprint arXiv:1911.05944, 2019.
- [28] F. Sun, C. Wang, L. Gong, C. Xu, Y. Zhang, Y. Lu, X. Li, and X. Zhou, "A power-efficient accelerator for convolutional neural networks," in 2017 IEEE International Conference on Cluster Computing (CLUSTER). IEEE, 2017, pp. 631–632.
- [29] X. Glorot and Y. Bengio, "Understanding the difficulty of training deep feedforward neural networks," in Proceedings of the thirteenth international conference on artificial intelligence and statistics, 2010, pp. 249–256.
- [30] J. Jihong, "Caffe initializers," <https://jihongju.github.io/2017/05/10/caffe-filler/>, May 2017.
- [31] M. L. Mastery, "Why initialize a neural network with random weights?" <https://machinelearningmastery.com/why-initialize-a-neural-network-with-random-weights/>, May 2017.
- [32] M. Yedroudj, F. Comby, and M. Chaumont, "Yedroudj-net: An efficient cnn for spatial steganalysis," in 2018 IEEE International Conference on Acoustics, Speech and Signal Processing (ICASSP). IEEE, 2018, pp. 2092–2096.
- [33] A. Pro, "Image histogram," <https://pro.arcgis.com/en/pro-app/help/analysis/geoprocessing/charts/image-histogram.htm>.
- [34] Wikipedia, "Normal distribution," https://en.wikipedia.org/wiki/Normal_distribution.
- [35] Y. LeCun, L. Bottou, Y. Bengio, and P. Haffner, "Gradient-based learning applied to document recognition," Proceedings of the IEEE, vol. 86, no. 11, pp. 2278–2324, 1998.
- [36] "Random number generation using lfsr," <https://www.maximintegrated.com/en/design/technical-documents/app-notes/4/4400.html>, accessed: 2021-01-24.

VIII. AUTHORS BIOGRAPHY



TOLULOPE A. ODETOLA received his Bachelors degree from Obafemi Awolowo University Nigeria in Electronic and Electrical Engineering. He received his Masters degree in Electrical and Computer Engineering from Tennessee Technological University, Cookeville, TN, USA. He is currently pursuing his Doctorate degree in Tennessee Technological University. He developed hardware/software co-verification techniques for CNN deployments on hardware accelerators. His current research interest includes FPGAs, hardware security, IoT security, machine learning, and deep learning.



FAIQ KHALID (GS'18-M'21) received his M.S. degree in electrical engineering and his B.E. degree in electronics engineering from the National University of Sciences and Technology (NUST), Pakistan, in 2016 and in 2011, respectively. He is currently pursuing his Ph.D. degree in hardware security and machine learning security at Technische Universität Wien (TU Wien), Vienna, Austria. He is a recipient of the Quaid-e-Azam Gold Medal for his academic achievements and the Richard Newton Young Fellowship Award at DAC 2018. His research interests include formal verification of embedded systems, hardware design security, and security for machine learning systems. He has also served as a TPC member of FIT, WSAV, ARES and ICONS.



TRAVIS SANDEFUR received his Bachelors in Electrical and Computer Engineering from Tennessee Technological University, Cookeville, TN, USA. He is currently pursuing his masters in Electrical and Computer Engineering also in Tennessee Technological University. His currently working on techniques for object detection on resource constrained devices. His current research interest includes FPGAs, machine learning, partial reconfiguration and deep learning.



HAWZHIN MOHAMMED received his B.Sc. degree in electrical engineering from Salahaddin University, Erbil, Iraq, in 2000. He received his M.Sc. degree from Tennessee Technological University, Cookeville, TN, USA, in 2017, where he is currently pursuing his Ph.D. degree at the Department of Electrical and Computer Engineering. His current research interest includes wireless network security, hardware security, IoT security, machine learning, and deep learning.



SYED RAFAY HASAN received the B.Eng. degree in electrical engineering from the NED University of Engineering and Technology, Pakistan, and the M.Eng. and Ph.D. degrees in electrical engineering from Concordia University, Montreal, QC, Canada. From 2006 to 2009, he was an Adjunct Faculty Member with Concordia University. From 2009 to 2011, he was a Research Associate with the Ecole Polytechnique de Montreal. Since 2011, he has been with the Electrical and Computer Engineering Department, Tennessee Tech University, Cookeville, TN, USA, where he is currently an Associate Professor. He has published more than 69 peer-reviewed journal and conference papers. His current research interests include hardware design security in the Internet of Things (IoT), hardware implementation of deep learning, deployment of convolution neural networks in the IoT edge devices, and hardware security issues due to adversarial learning. He received SigmaXi Outstanding Research Award, Faculty Research Award from Tennessee Tech University, the Kinslow Outstanding Research Paper Award from the College of Engineering, Tennessee Tech University, and the Summer Faculty Fellowship Award from the Air force Research Lab (AFRL). He has received research and teaching funding from NSF, ICT-funds UAE, AFRL, and Intel Inc. He has been part of the funded research projects, as a PI or a Co-PI, that worth more than \$1.1 million. He has been the Session Chair and Technical Program Committee Member of several IEEE conferences including ISCAS, ICCD, MWSCAS, and NEWCAS, and a Regular Reviewer for several IEEE Transactions and other journals including TCAS-II, IEEE ACCESS, Integration, the VLSI Journal, IET Circuit Devices and Systems, and IEEE Embedded System Letters.